Smart Agricultural Technology 6 (2023) 100347

Contents lists available at ScienceDirect

Smart Agricultural Technology

journal homepage: www.journals.elsevier.com/smart-agricultural-technology

Mapping sugarcane residue burnt areas in smallholder farming systems using machine learning approaches

Koutilya PNVR [a], Varaprasad Bandaru [b,*]

[a] Department of Electrical & Computer Engineering, University of Maryland, MD, United States
[b] USDA-ARS, Maricopa, AZ, United States

ARTICLE INFO

Keywords:
Support vector machines
Neural networks
Sentinel-1 SAR
Harmonized Landsat Sentinel-2 data
Land cover mapping

ABSTRACT

Satellite remote sensing methods have been proven to quantify the burnt areas resulting from different fire activities reliably. However, they were reported to perform poorly to identify crop residue burnt areas, particularly in smallholder systems due to lack of frequent and high spatial resolution satellite data. In this study, we used Harmonized Landsat Sentinel-2 (HLS) observations and evaluated two machine learning classifiers (i.e., Support Vector Machines (SVM) and Artificial Neural Networks (ANN)) to map sugarcane burnt areas for the 2019–20 season in a smallholder farming region in Thailand.

Results showed that both classifiers performed well in identifying the spatial patterns of sugarcane burnt areas in the region. The ANN outperformed SVM at both pixel and regional scales. At pixel level, ANN accuracy was 93.4 % while SVM's best-performing Polynomial kernel accuracy was 82.7 %. The ANN estimated average percent burnt area (51.1 %) in the region was closer to reported value (48.7 %) by Thailand's Office of Cane and Sugar Board (OCSB), compared to the SVM estimate (62.9 %). The total estimated burnt areas by ANN and SVM (315 and 418 thousand ha, respectively) deviated more from OCSB's area (240 thousand ha) compared to percent burnt area. However, area estimates from classifiers had significantly better accuracy than the estimates of MODIS burnt products.

Overall, this study demonstrated that HLS observations provided required spectral information to build promising models to map burnt areas in smallholder systems with higher accuracy than global products. Our mapping algorithm using the ANN classifier showed the potential to monitor sugarcane burnt areas reliably, and contribute to the successful implementation of regulatory policies in Thailand.

Introduction

In many of the leading sugarcane producing countries, such as Brazil, India, China, Thailand and the United States of America, burning of crop residues, either pre- or post-harvest, has been a common practice [1]. Air pollutants (e.g., particulate matter) resulting from crop residue burning are found to cause serious human health problems [2]. In addition, they change the composition of the atmosphere and contribute to global climate change by affecting the radiation balance. Furthermore, sugarcane residue burning negatively impacts soil quality by causing the loss of soil organic carbon, nutrients and erosion, which, in turn, can have long-term implications for food production [3].

Due to serious human health and environmental concerns, there have been efforts to control sugarcane residue burning through placing regulatory policies. For example, the Thailand government introduced Green Cane Purchasing policy, starting in the 2019–20 to restrict sugarcane mills to purchase 30 % of the burnt cane in their total purchases and it is further tightened, limiting burnt cane purchases to 20 % starting from the 2020–21 season [4]. Similarly, in the State of São Paulo, one of the major sugarcane regions in Brazil, a legislation (Law N∘11.241/2002) was introduced to gradually eliminate the burning practice by 2031 [5]. Moreover, there have been various attempts, with varying success, to improve emission inventories associated with crop residue burning that can inform policies and help develop mitigation strategies [6].

Accurate mapping of burnt areas is essential for assessing the impacts of regulations on controlling burning. Additionally, it is necessary for accurately determining biomass emissions using bottom-up approaches to improve emission inventories, which are required for climate studies to understand the emission impacts on climate.

* Corresponding author.
E-mail address: prasad.bandaru@usda.gov (V. Bandaru).

https://doi.org/10.1016/j.atech.2023.100347
Received 12 May 2023; Received in revised form 21 October 2023; Accepted 22 October 2023
Available online 23 October 2023

Satellite remote sensing has been widely used to develop methods for identifying active fires and burnt areas [7,8]. Algorithms developed for identifying active fires primarily rely on thermal anomalies (i.e., difference in brightness temperatures between potential fire and land cover around it) [9]. The brightness temperatures are determined using radiances from thermal infrared bands (e.g., 10–11 μm). In contrast, burnt area mapping algorithms use differences in surface reflectance and/or spectral indices such as Burn Area Index (BAI) and the Normalized Burn Ratio (NBR)) to distinguish between burnt and no-burnt areas [10,11].

There are operational global products for both active fires (MOD14/MYD14 and VNP14) and burnt areas (MCD64A1), produced using MODIS and VIIRS data [7]. Previous studies have consistently reported poor performance of these products in identifying burnt areas in croplands, particularly in smallholder farming systems, where fields are smaller than 10 ha ([6,8,12,13]). Several factors contribute to this poor performance. Firstly, cropland fires are often short-lived, and satellite overpass times often do not match fire activity, making it challanging for satellite observations to capture active fire signals. Secondly, the course resolution (≥250 m) of these satellite instruments may not capture changes in spectral characteristics due to the small field sizes and the heterogeneity of croplands in smallholding systems. Finally, the land cover maps used to produce these operational global products only include broad cropland classes, lacking crop type maps, which are necessary for accurate determination of harvesting timing of individual crops.

Recent advances in satellite remote sensing, such as Harmonized Landsat and Sentinel-2 (HLS) data [14], combine Landsat 8 and Sentinel-2 satellite observations to produce frequent optical observations, typically every 4–8 days. These frequent, high-resolution observations enable the identification of the changes in crop-specific characteristics with harvesting and burning events, allowing mapping of burnt and non-burnt areas resulting from crop residue burning in smallholding farming systems.

Recently, machine learning approaches have been widely explored to map burnt areas. Unlike rule-based methods, machine learning approaches have the ability to learn the characteristics of burnt pixels from labeled training samples. Previous studies have employed various machine learning approaches, such as random forests [15–17], support vector machines[18–20] and neural networks [17,21–25], for burnt area mapping. However, there have been limited studies on the applicability of machine learning approaches for mapping burnt areas resulting from agricultural fires, particularly in smallholder farming systems. To the best of our knowledge, there are no studies on exploring the use of machine learning for sugarcane residue burnt area mapping.

Given the need for a reliable method to map sugarcane crop residue burnt areas, this study aims to evaluate the performance of two machine learning approaches in mapping sugarcane residue burnt areas in smallholder systems in Thailand for 2019–20 growing season, using HLS satellite observations. Firstly, we generated a land cover map with crop types, including sugarcane, at a high spatial resolution (30 m) using Sentinel-1 Synthetic Aperture Radar (SAR) imagery. Next, we extracted sugarcane pixels from the land cover map and used them to retrieve corresponding satellite observations over the growing season from HLS data. These satellite observations, along with field observations of burnt and non-burnt areas, were used to develop mapping algorithms based on Support Vector Machines (SVM) and Neural Networks (NN). These algorithms were implemented within a dominant smallholder farming region in Thailand. We choose SVM and NN classifiers as they represent separate groups of machine learning classifiers. SVM, similar to random forests, is a conventional classifier. We used SVM as a baseline to understand whether there is enough information in the raw multispectral bands to classify burnt areas. Neural networks, on the other hand, belong to a more powerful family of classifiers, and we used to assess their performance in improving mapping accuracy compared to the SVM method.

Study region

The study region is located in the central and northeast parts of Thailand (Fig. 1). It occupies six provinces. This region represents a dominant region of sugarcane cultivation, producing about 38 % of the total Thailand sugarcane production. The planting area of sugarcane is approximately 1.2 million ha. Most of the sugarcane cultivation area is rainfed (about 90 %) [26], and more than 80 % of the sugarcane in this region is cultivated on small farms with area less than 10 ha [27]. In this region, there are nine sugar mills. Other major crops cultivated in this area include rice, cassava, and maize.

Brief description of the classifiers

Support vector machines (SVMs)

Support Vector Machines are a class of supervised classifiers based on statistical learning theory [28–30]. For a baseline configuration of binary classification, let the training dataset has N samples x1, x2,…, xN with corresponding labels y1, y2,...., yN where yi E {−1, 1} for $i = 1, 2,..,$ N. A simple linear SVM classifier for such a setting finds an optimal hyperplane W among many possible solutions by maximizing the margin defined as the sum of distances between the hyperplane and nearest positive and negative examples. So, the mathematical form of a Linear SVM hyperplane classifier can be represented with the following equation.

$$W.X - b = 0$$

Where b is an offset of this hyperplane from the origin; W is a parameter that determines the orientation of the hyperplane and X can be any point lying on this hyperplane.

Assuming this data is linearly separable, SVM finds the maximum-margin hyperplane that maximizes the margin defined to be the distance between two hyperplanes parallel to the original classifier containing the positive and negative training samples. As shown in Fig. 2, the training samples that lie on these parallel hyperplanes are called support vectors. So the goal of SVM is to find the hyperplane that maximizes the marginal distance between the hyperplanes containing the positive and negative support vectors.

W.Xi - b >= 1 for all points X belonging to positive class yi=1 (equality holds true for support vectors)
W.Xi - b <= −1 for all points X belonging to negative class yi=−1 (equality holds true for support vectors)
Combining the above two, yi*(W.xi - b) >= 1 for all training samples 1<= i <= N.

Geometrically the margin distance between these two hyperplanes containing the support vectors is 2/||W||, thus the goal would be to minimize ||W||. To sum up a simple linear SVM optimization problem can be written as follows:

Min ||W||
Such that yi*(W.xi - b) >= 1 for 1 <= i <= N

However, for a complex training data distribution where the data is not linearly separable, we can extend a similar concept of LinearSVM but after transforming the data into a higher dimensional space where the data becomes linearly separable. Such a projection of data into a higher dimensional space can be achieved through kernel functions such as RBF kernel, polynomial kernel and sigmoid kernel.

In our work, we used SVM with various kernels as the baseline to get the burnt mapping classification performance and understand the raw information present in the data. Then we compared it with Neural Network to better understand the power and capacity of these classifiers for mapping burnt areas.

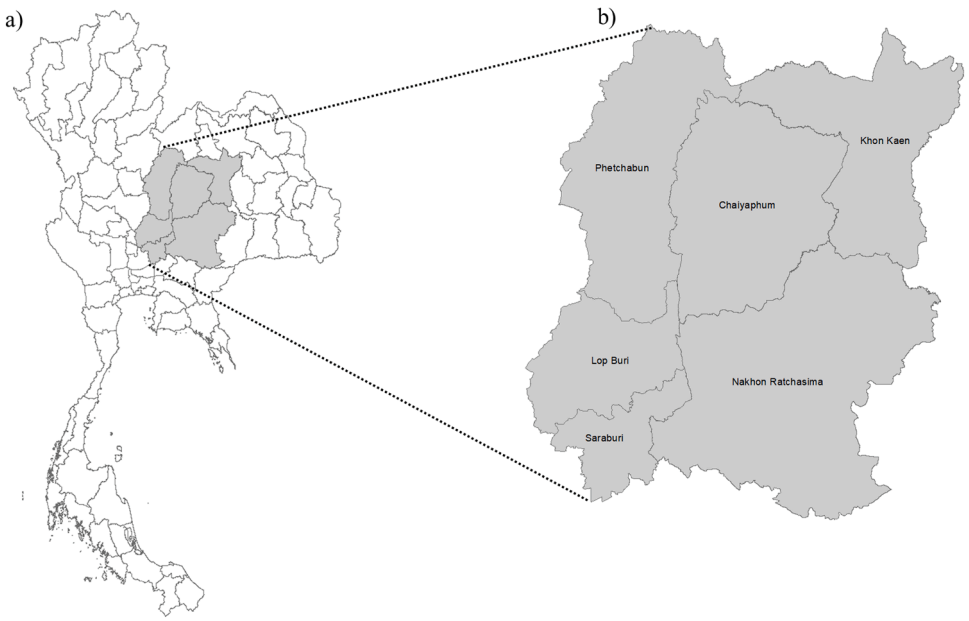

Fig. 1. (*a*) Map of the Thailand and (*b*) study region comprising six provinces.

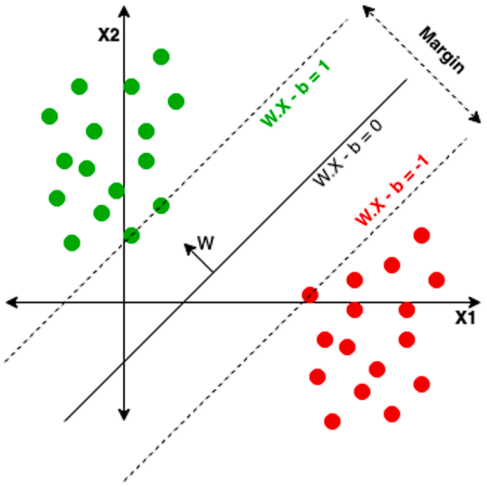

Fig. 2. An illustration of a typical Linear SVM classifier for binary classification.

Neural networks

Neural Networks (NN) are a more powerful set of supervised classifiers compared to SVM. NNs are an extension of Multilayer perceptron networks [31,32] that is inspired from the neural modeling of the brain, mimicking the way that biological neurons signal to one another. They contain various layers starting with an input layer followed by a set of hidden layers and ending with an output layer. Non-linear activations at every hidden layer makes the neural networks capable of handling non-linear data. Neural networks rely on the back-propagation algorithm to update its state (parameters) to fit the training data better with each iteration of training.

The core idea of Neural Networks has shown tremendous amounts of improvements in several tasks of Computer Vision [33], Natural Language Processing [34], speech processing [35] and many more areas. Many remote sensing applications also started to take advantage of these powerful classifiers in their methods such as preseason crop mapping [36]. The architectural design of our NN was shown in Fig. 3 and details of the NN model was provided in the implementation Section 5.1.

Data sources and preparation

The datasets required to develop classifiers and map sugarcane burnt areas include: 1) a sugarcane mask to identify the sugarcane pixels, 2) field observations for training and validation, and 3) satellite observations as predictive variables. Fig. 4 illustrates the steps involved in preparing the data for the development and implementation of classifiers. In Step 1, a sugarcane mask (30 m) was created based on the 2019 land cover map produced using Sentinel-1 SAR data and Long Short-Term Memory (LSTM) deep neural network algorithm. In Step 2, harmonized Landsat 8 and Sentinel 2 (HLS) satellite observations [14] for nine spectral bands during sugarcane harvesting period were extracted for each harvested non-green sugarcane pixel using the sugarcane mask. In Step 3, HLS observations were extracted for burnt and non-burnt sugarcane field locations collected using wind-shield surveys in the study region. These observations were used for training, validation, and testing of NN and SVM models. In Step 4, the models were implemented over the sugarcane pixels using HLS observations and mapped sugarcane burnt and non-burnt areas for the 2019–20 growing season. The data sources and preparation steps are described in detail below.

Sentinel-1 SAR satellite data

The fundamental requirement for mapping post-fire burnt areas is the availability of a crop type mask to identify the location of sugarcane pixels. To produce a high-resolution land cover map that includes sugarcane, we used Sentinel-1 Synthetic Aperture Radar (SAR) imagery. Sentinel-1, a constellation of two satellites operating in a near-polar, sun-synchronous orbit, offers a 6-day local repeat pass with several modes, including the interferometric wide swath (IW) mode that we used for land cover mapping. We acquired a full time series stack of 53 images for the year 2019 covering the study region from the Alaska Satellite Facility. The ground-range detected images were pre-processed using the SNAP Sentinel-1 toolbox. The pre-processing steps included orbit correction, thermal noise removal, radiometric calibration to correct for viewing geometry effect, terrain correction using NASA Shuttle Radar Topography Mission (SRTM) 30 m data [37], and speckle-noise filtering to reduce constructive and destructive interference. The images were then converted from linear values to logarithmically scaled values in decibels, resulting in VV and VH polarized imagery with

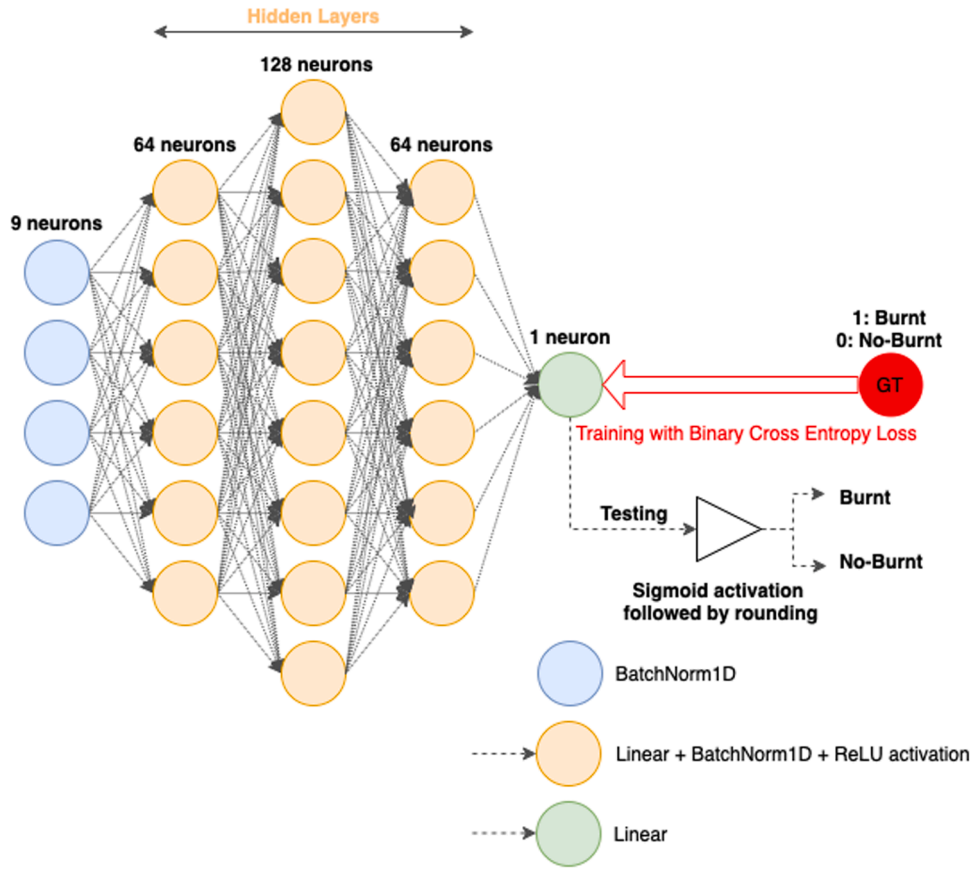

Fig. 3. Architecture of the Neural Network (NN) used for burnt area mapping. The NN model was designed with 9 nodes, representing reflectance of 9 spectral bands in the sentinel-2 data, and 3 hidden layers with 64, 128 and 64 nodes respectively with ReLU non-linear activation and ending with an output layer with one node for our binary classification prediction.

sigma-nought backscatter values in decibels [8].

Sugarcane mask

Sugarcane mask was generated using the 2019 land cover map of the study region (Fig. 4). Firstly, a land cover map including sugarcane cultivated during the 2019–2020 growing season was produced using the sigma-nought backscatter values of sentinel-1 VV and VH polarized imagery and elevation data. The elevation data was extracted for the study region using NASA SRTM data [37]. We employed the Long Short-Term Memory (LSTM) deep neural network algorithm in Pytorch [36].

To create the model, we used available Sentinel-1 images to produce a sequence of 7-day composites resulting in 53 composite images with three bands (VV, VH, and elevation). For developing the model, we created labels with different land cover types for 1700 field polygons. These field polygons were intercepted with Sentinel-1 data to create a total of 50,450 training (70 %), validation (20 %), and testing (10 %) labeled pixels.

The model was trained as a four-layered LSTM on the training and validation set. The final accuracy of the model was generated based on predictions on test data. Furthermore, the model was implemented over the study region, and sugarcane pixels were extracted to create a mask. The overall accuracy of the sugarcane mask is approximately 91 % (Fig. 5).

Harmonized Landsat Sentinel (HLS) satellite data

The classification methods we developed used harmonized Landsat 8 and Sentinel 2 (HLS) observations from nine available spectral bands as predictive variables [14]. The HLS dataset provides radiometrically harmonized surface reflectance imagery from the Operational Land Imager (OLI) instrument onboard Landsat 8 and the MultiSpectral Instrument (MSI) onboard Sentinel-2A and Sentinel-2B. Combined imagery from these instruments produces time series observations with a frequency of 1–4 days at a spatial resolution of 30 m. Both Landsat and Sentinel imagery were treated with consistent atmospheric correction, cloud screening, geolocation, normalization of illumination and view angles, and spectral bandpass adjustments across sensors [38].

We acquired available HLS data (a total of 29 images) from December 1, 2019, to March 31, 2020, during the crop residue burning and harvesting season. The HLS dataset includes quality assurance (QA) data with flags identifying the occurrence of clouds, cloud shadows, and snow. Using the QA layer, we removed pixels with clouds, cloud shadows, and snow.

Preparation of HLS data

The HLS surface reflectance data of sugarcane pixels are required for developing and implementing model for burnt area mapping. The sugarcane map was projected to the same projection as HLS reflectance data (i.e., WGS 84 / UTM zone 47 N coordinate system). Then both sugarcane map and HLS data were overlaid with each other and extracted HLS reflectance data for all the bands corresponding to each sugarcane pixel. After harvesting without burning or burning, fields are expected to have no green pixels. Presence of green pixels indicates that either crop is still in the maturing stage and not harvested or the following crop is germinated. To remove green pixels in the HLS time series, we computed Normalized Difference Vegetative Indices (NDVI) and removed pixels that have NDVI greater than 0.3 as they are considered as green pixels.

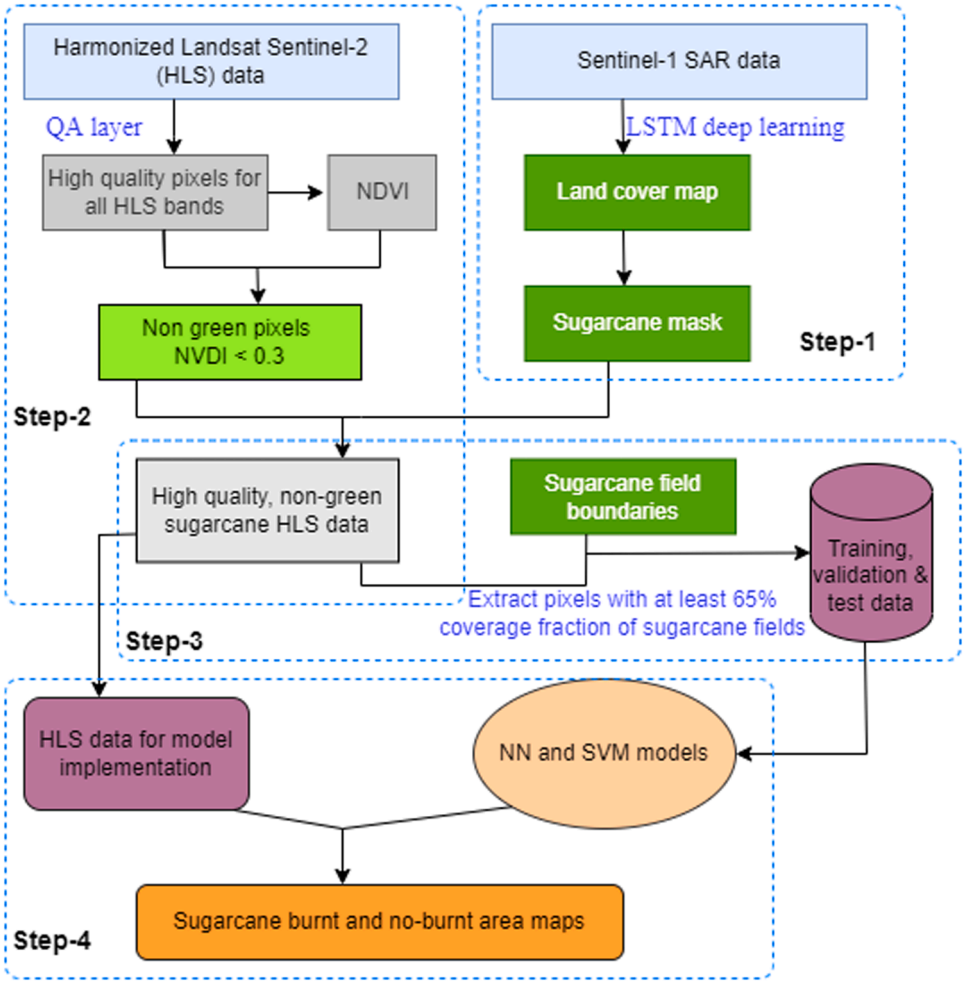

Fig. 4. Schematic illustrating steps for HLS data preparation for model development and implementation.

These HLS observations for non-green pixels obtained during the burning and harvesting period of sugarcane were used for development and implementation of models.

Training, validation, and test data

To train both SVM and NN classifiers and test their performance, we conducted windshield surveys during harvesting season of 2019–20 growing season and collected information on residue management practices from 480 sugarcane fields across the study region (Fig. 6). Using these fields, the total of 22,000 sample pixels (30-m), by intersecting with sugarcane mask. We considered 81 % of the total samples for training the classifiers, 9 % as the validation set to select the best model, and 10 % as a test set to report testing performance for the trained models. When sampling, pixels that had 65 % of the total fraction covering the fields, to ensure that HLS data used in developing models reflects spectral properties of sugarcane fields.

Development and implementation of the models

NN based method

We used the pytorch framework in python to define, train and develop a NN method. As shown in Fig. 3, we defined a NN with 9 nodes, representing reflectance of 9 spectral bands in the sentinel-2 data, and 3 hidden layers with 64, 128 and 64 nodes respectively with ReLU non-linear activation and ending with an output layer with one node for our binary classification prediction. We also used batchnorm [] at every layer except for the final output layer. To sum up, the architecture was designed as follows: [Linear(9, 64), BatchNorm, ReLU], [Linear(64, 128), BatchNorm, ReLU], [Linear(128, 64), BatchNorm, ReLU], [Linear (64, 1)]; where Linear(M, N) is a fully connected network connecting two layers with M and N nodes respectively. To train this NN, we used BCEWithLogitsLoss (BinaryCrossEntropy for Logits loss) from the pytorch package along with Adam's optimizer and a learning rate of 0.001. We trained this NN for 5000 epochs.

SVM based method

We used the scikit-learn package in Python to develop an SVM-based method. The package offers inbuilt kernel functions such as Linear, RBF, polynomial, and sigmoid which we utilized. We used the raw band values as input and trained different SVMs on different kernels on the {train+val} dataset. We then reported the testing performance by implementing the method on the test set. Since the SVM's feasibility is being studied, default parameters were used. For instance, C (regularization) was set to 1.0, and gamma was scaled internally based on the variance of the training samples.

Implementation of models

Both NN and SVM trained models were implemented on pre-processed HLS time series data of sugarcane pixels, covering the whole study region, and estimated burnt and no-burnt sugarcane pixels

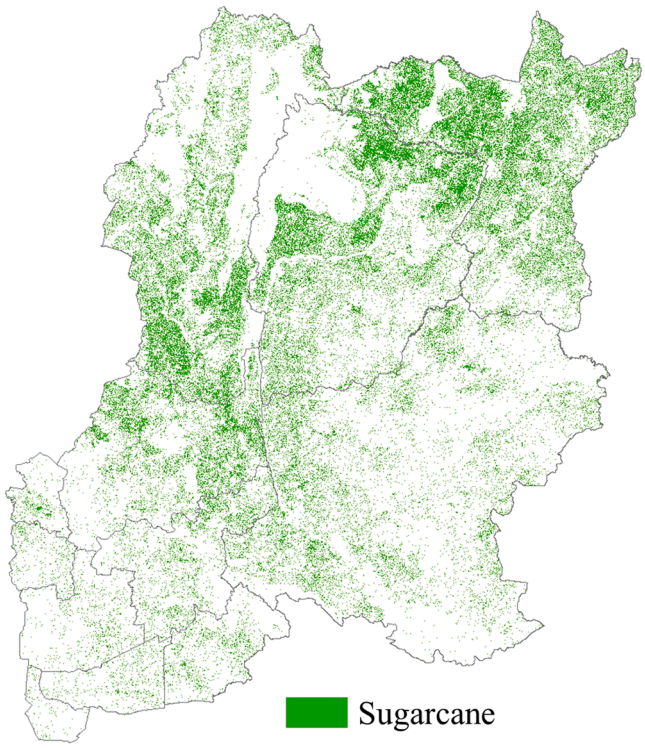

Fig. 5. Sugarcane mask (30 m) produced using 2019 land cover map developed using LSTM deep neural network algorithm and sentinel-1 SAR data.

during the harvesting period from December 01, 2019 to March 31, 2020.

Accuracy assessment

Pixel level evaluation

The performance of the NN and SVM-based methods was evaluated at both pixel and regional scales. For pixel-level evaluation, we used the test data, while regional-scale performance was assessed using Thailand's Office of Cane and Sugar Board (OCSB) reports on provincial-level sugarcane production by harvesting practices.

At the pixel level, for the SVM-based method, we obtained the maximum-margin hyperplane parameterized by W and b. All pixels in the test set were classified based on their location on the hyperplane, and classification was computed as the ratio of the number of pixels correctly classified over the total number of pixels in the test set.

For the NN-based method, pixel-level performance was evaluated at two steps. Firstly, validation was performed on the validation data during model development. During this process, as the model was trained for 5000 epochs, we measured the validation accuracy at regular intervals by feeding validation pixels to the trained NN model. We used a sigmoid activation function to squash the NN predicted output between 0 and 1, and applied a threshold of 0.5 to classify them as burnt (1) or no-burnt (0). Once the model with the best validation performance was selected, we implemented it over the pixels in the test data and assessed classification accuracy using the confusion matrix (Fig. 7C).

To evaluate the statistical significance and superiority of one classifier compared to the other, we used McNemar's test [39]. McNemar's test is a parametric test based on the chi-squared distribution ($\chi 2$). It tests the null hypothesis that the two classifiers have equal performance.

$$\chi 2 = (f_n - f_m)^2 / (f_n + f_m) \quad (1)$$

where f_n represents the number of observations that classifier one incorrectly classified but classifier two correctly classified, and f_m rep-

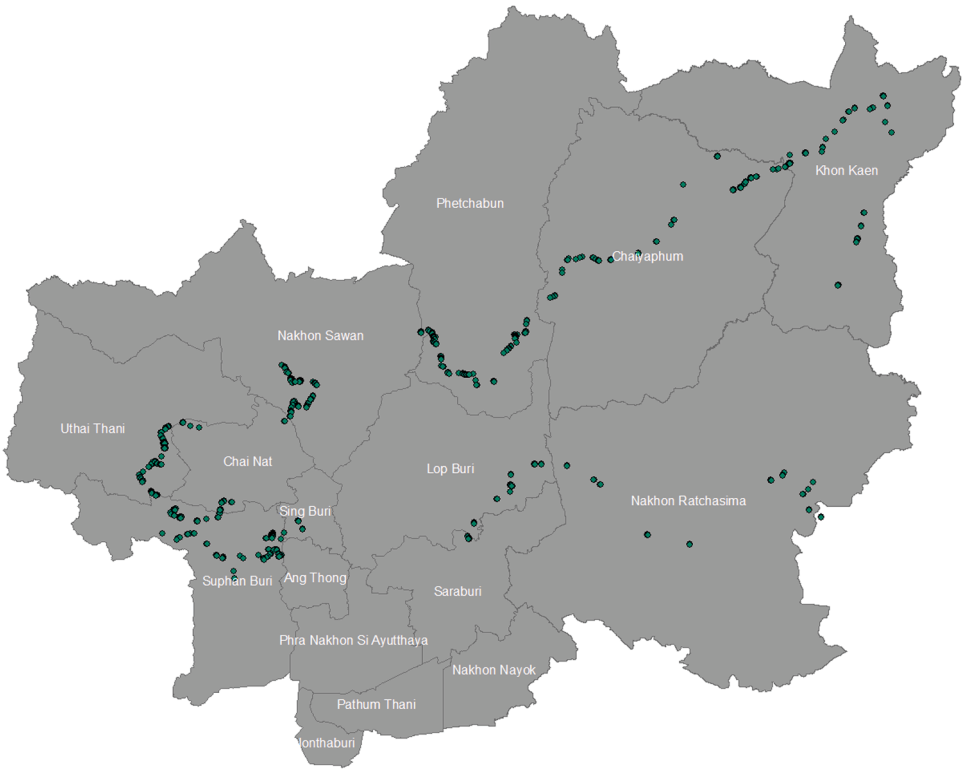

Fig. 6. Green filled circles represent locations of burnt and no-burnt sugarcane fields. These field coordinates were collected using windshield surveys.

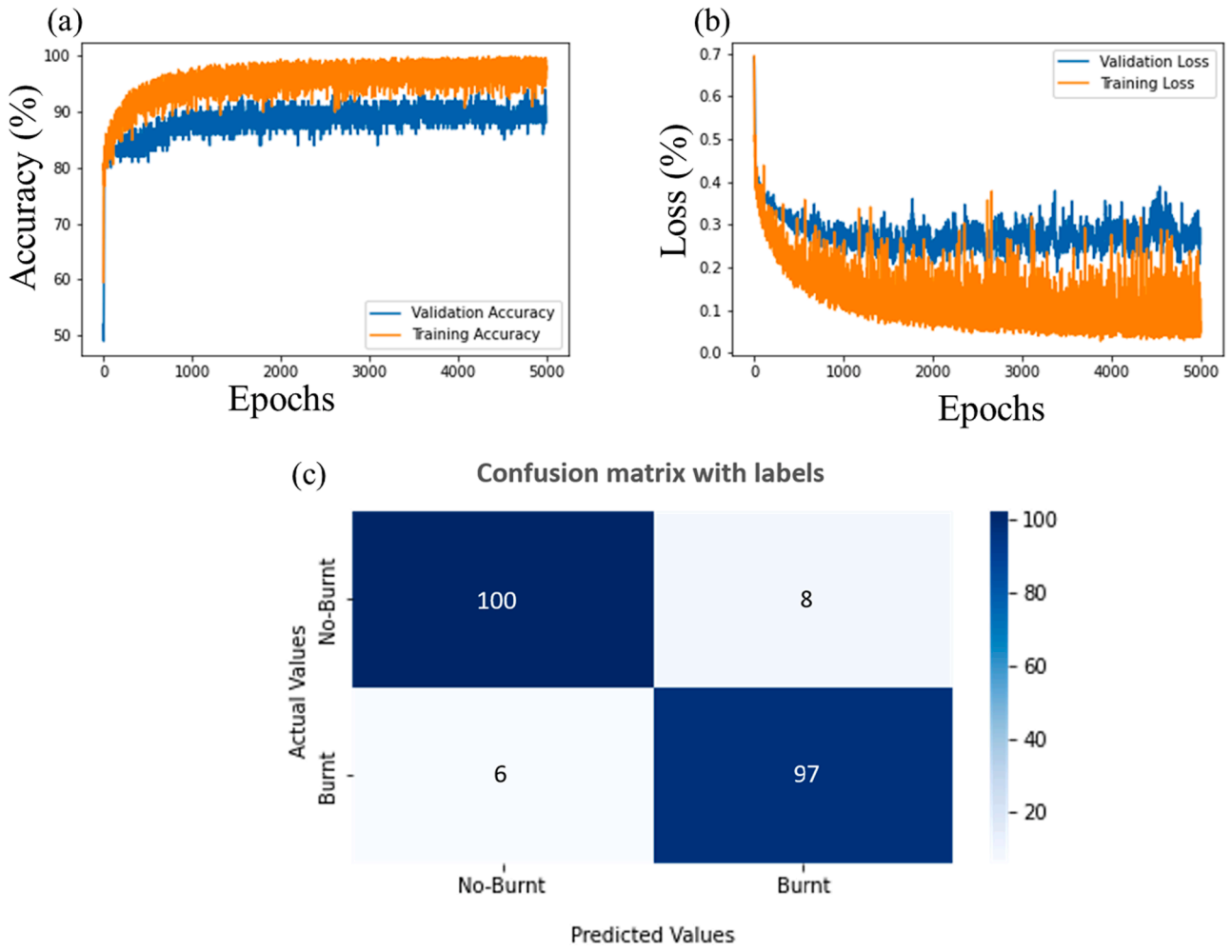

Fig. 7. (*a*) Training and Validation Accuracies, (*b*) Training and Validation Losses (*c*) Confusion Matrix on the test data.

resents the number of observations that classifier one correctly classified but classifier two wrongly classified.

In addition, to understand the performance of both classifiers in terms of burnt area detection accuracy, we computed three performance metrics described by Kontoes et al. [40]. These include detected area efficiency (DAE), skipped area rate (SAR, omission error) and false area rate (FAR, commission error). These metrics were computed using following formulae:

$$\text{Detection Area Efficiency (DAE)} = \frac{\text{DBA}}{\text{DBA} + \text{SBA}} \tag{2}$$

$$\text{False Area Rate (Commission Error)} = \frac{\text{FBA}}{\text{DBA} + \text{FBA}} \tag{3}$$

$$\text{Skipped Area Rate (Ommission Error)} = \frac{\text{SBA}}{\text{DBA} + \text{SBA}} \tag{4}$$

Regional scale evaluation

The regional scale performance of the NN and SVM methods were assessed by comparing them with OCSB reports (Office of Cane and Sugar Board [41]) for the 2019–20 sugarcane harvesting period. The OCSB provides data on total procured sugarcane by practice (i.e., fresh sugarcane that is not burnt and burnt sugarcane) at each sugarcane processing unit in Thailand for every year. Typically, sugarcane is cultivated in the vicinity of the sugarcane processing unit. Each province where sugarcane is cultivated, has 1–3 sugarcane processing units. We aggregated the total procured sugarcane at processing units in each province and this total was considered as provincial level sugarcane production by practice. Using fresh and burnt cane production, we computed percent burnt area and total burnt area in hectares by province. Similarly, we aggregated all the classified pixels, using NN and SVM methods, in the study region by practice and by province. These provincial level aggregated estimates were compared with OCSB based percent burnt area and total burnt area and estimated absolute percentage error.

Results and discussion

Pixel level performance

Performance of NN classifier

Two-level performance assessment was conducted: (1) validation during model development and (2) validation after implementation. The training and validation accuracies and losses over the training period are shown in Fig. 7. It can be observed that as the training progressed with epochs, the training loss was reduced, and the accuracy increased to almost 100 %, indicating that the NN classifier learned to fit the training data accurately. A similar curve pattern for validation loss and accuracy implies that the NN is able to generalize its performance when implemented over a large region by matching the pattern in the training curves. The best validation accuracy was observed to be 93 % at epoch 3393. We used this best model to evaluate the performance at a regional scale using the test data. The results showed that the test accuracy of the

final model is 93.43 %

Performance of SVM classifier

Results indicated that all kernel functions except sigmoid kernel performed reasonably well with accuracy greater than 80 %. Polynomial and Radial Basis Function (RBF) kernels performed the best with approximately same accuracy (Polynomial=81.2 % & RBF=79.8 %) SVM performed the best with accuracy of 81.2 %, followed by Linear kernel (80.2 %). The performance of the sigmoid kernel (28.6 %) is significantly inferior compared to the other three. The Polynomial and RBF kernels project the training data into a higher dimensional space where finding a classifier hyperplane is relatively more successful than finding one in the original space offered by the Linear and Sigmoid kernels. Similar findings were reported in the previous studies focusing on land cover classification [42,43].

These results indicated that the SVM classifiers underperformed relative to the NN classifier, which was confirmed by results of McNemar's test and burnt area detection accuracy metrics.

As shown in a two by two contingency table (Table 1), of the total 213 fields compared for accuracy assessment, NN method classified 147 fields correctly which were wrongly classified by SVM. Whereas NN classified 9 fields incorrectly that were classified correctly by SVM. Both methods classified 52 correctly and 5 fields incorrectly. McNemar's test suggested a chi-square test statistic value of 122 which exceeded the chi-square critical value of 3.84 (alpha=0.05). Therefore, the null hypothesis that both the NN and the SVMs were equal in performance was rejected and the relatively higher superiority of the NN method over SVM was accepted.

As shown in Table 2, the NN method has considerably higher burnt area detection efficiency and lower skipped area rate and lower false area rate compared to the SVM method.

The possible reasons for lower performance of SVM method could be the number of training samples and input variables used in the training. Previous studies comparing SVM and NN for classification reported that SVM outperformed or equally compared to NN when training samples are fewer [44]. However, as the number of training samples increased, NN was found to outperform SVM method. Li et al. [45] reported higher accuracy with NN method with relative to SVM to predict active fires when used approximately 20,000. In our study, about 18,000 samples were used in the training which appeared to be optimal for NN to achieve better performance over SVM. Similarly, the number of explanatory variables used in the training also impacts the performance of SVM methods. Higher the number of explanatory variables, better the accuracy achieved with SVM approaches. Previous studies found that NN methods performed better over SVM with sub-optimal number of explanatory variables [46]. We used nine spectral bands as input variables which might be sub-optimal for SVM to perform equally to NN method.

Comparison of regional scale performance

The burnt area maps generated by the NN and SVM classifiers and their spatial patterns are illustrated in Fig. 8a & b. Although the number of burnt pixels in the SVM map was considerably higher (Fig. 8c), the spatial patterns of both maps were found to be consistent. For instance, the southwest provinces of the study region had higher burnt pixels compared to the northeast provinces. As shown in Fig. 8a & b, the percentage of burnt area in Lop Buri and Sara Buri provinces, which are in the southwest part of the study region, was 71.10 % (SVM estimate=82.80 %) and 55.93 % (SVM estimate=68.72 %), respectively. On the other hand, Chaiyaphum and Khon Kaen provinces in the northwest region were estimated to have lower burning percentages, 42.21 % (SVM estimate=56.01 %) and 41.04 % (SVM estimate=46.46 %), respectively.

Table 1
Contingency table for the predictions from SVM and NN models on the test dataset.

	SVM (Correct)	SVM (Incorrect)
NN (Correct)	52	147
NN (Incorrect)	9	5

Table 2
Ratio of detected, skipped and false areas with respect to the ground-truth area for NN and SVM predictions on the test dataset.

	Detected Area Efficiency ↑	Skipped Area Rate (Omission Error)↓	False Area Rate (Commission Error)↓
SVM	43.6	56.31	67.6
NN	**94.1**	**5.8**	**7.6**

Comparison of NN and SVM estimates with OCSB reported numbers showed that the NN percent burnt area estimates are more closely aligned with OCSB reported values than SVM estimates (as shown in Fig. 9). The average NN and SVM-based percent burnt areas in the study region for the 2019–20 growing season were 51.08 % and 62.90 %, respectively, which were 4.86 % and 29.13 % higher than the OCSB percentage burnt area of 48.71 %. However, the absolute percentage error varies considerably among the provinces, ranging from 0.19 % to 19.59 % for NN estimates and from 13.34 % to 74.28 % for SVM estimates. The estimates for Chaiyaphum province exhibited the highest percentage error for both NN and SVM approaches. This could be attributed to the very low percentage burnt area reported for Chaiyaphum province by OCSB. OCSB reported only one sugarcane processing plant in Chaiyaphum province, and the reported burnt area for the 2019–20 growing season was 29 %, significantly lower than the average reported value for the study region.

Discrepancies in total areas

Although the burnt percentages were in good agreement with OCSB reports, particularly the NN approach, the area estimates were found to have higher uncertainties, regardless of the approach (Fig. 10). The total estimated burnt areas by the NN and SVM methods in the study region for the 2019–20 growing season were approximately 315 and 418 thousand ha, respectively, whereas the OCSB reported area was 249 thousand ha. The mean absolute percentage errors, estimated based on the OCSB report, were 26.99 % and 59.02 % for the NN and SVM estimates, respectively. The good agreement of percent burnt areas but discrepancies in the area estimates suggested that the area uncertainties originated from factors other than the SVM and NN classifiers. One such source of uncertainty is the sugarcane mask. The total sugarcane area estimated from the sugarcane mask was considerably higher than the OCSB reported sugarcane area, by 23 %.

Comparisons of global products

To understand the relative performance of SVM and NN classifiers for mapping burnt areas with reference to global products, we compared SVM- and NN-based products with two global burnt area products: a) the MODIS Terra and Aqua combined MCD64A1 Version 6 (500 m) burnt area product, and b) the MODIS FIRECCI51 (~250 m) burnt area product. The MCD64A1 is a monthly product produced using MODIS surface reflectance data (500 m) and active fire observations (1KM) [7]. The FIRECCI51 product is also a monthly product produced using Near Infrared Red reflectance from the MODIS reflectance product (250 m) and MODIS active fire data [47]. The global products were intersected with the sugarcane map to extract burnt sugarcane pixels and estimate the total burnt area in the region (Fig. 11).

The MCD64A1 and FIRECCI51 products estimated 46 and 67 thousand ha burnt area in the study region for 2019–20 growing season, respectively. These estimates were significantly lower than OCSB's

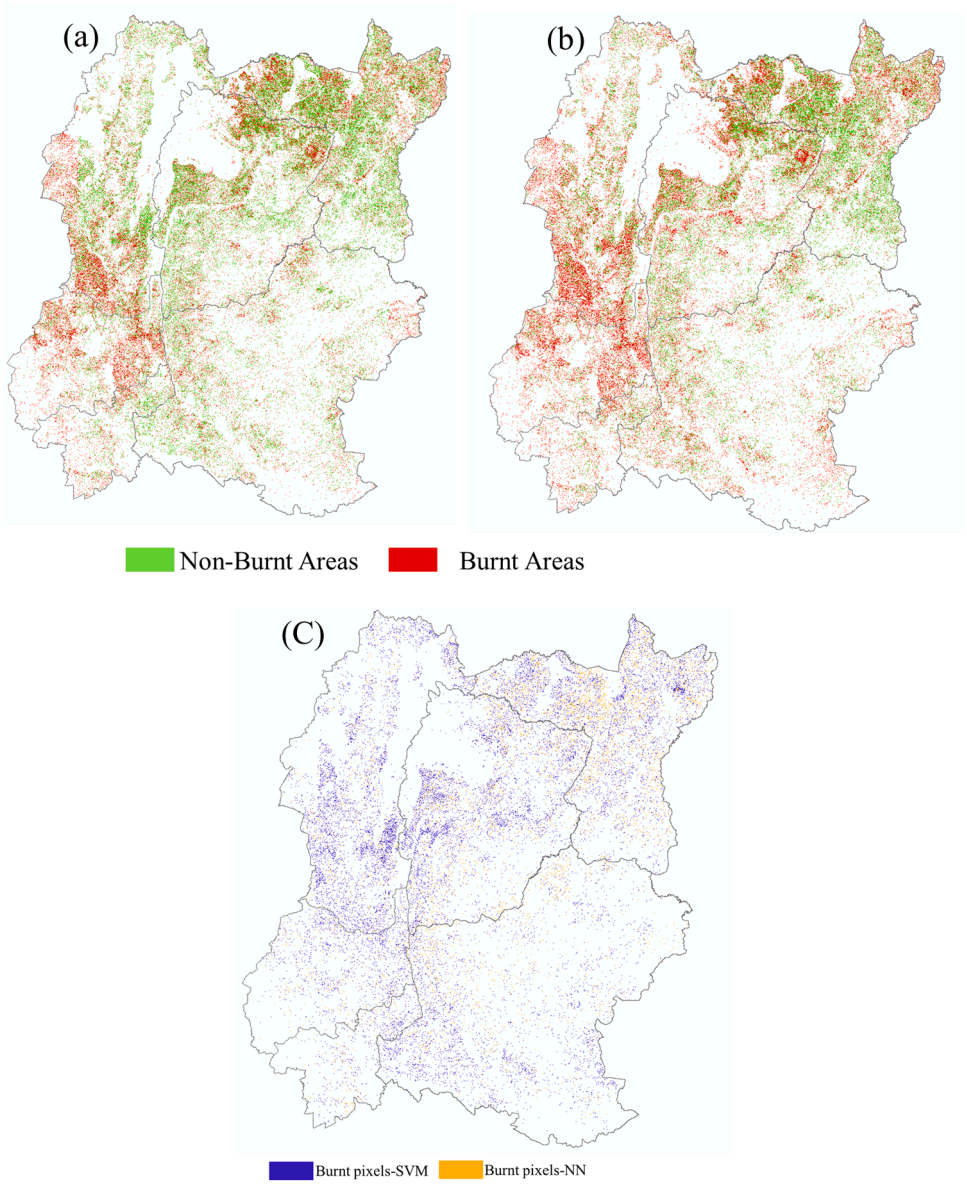

Fig. 8. Comparison of predicted burnt (red colored pixels) and no-burnt (green colored pixels) maps of neural network (NN) model (a) and support vector machines with polynomial kernel function (SVM) model (b). Difference between SVM and NN predicted burnt pixels (c), Burnt pixels-SVM represents pixels that SVM model predicted as burnt but NN model classified as no burnt while Burnt-NN indicates pixels that NN model classified as burnt but SVM model predicted as no burnt.

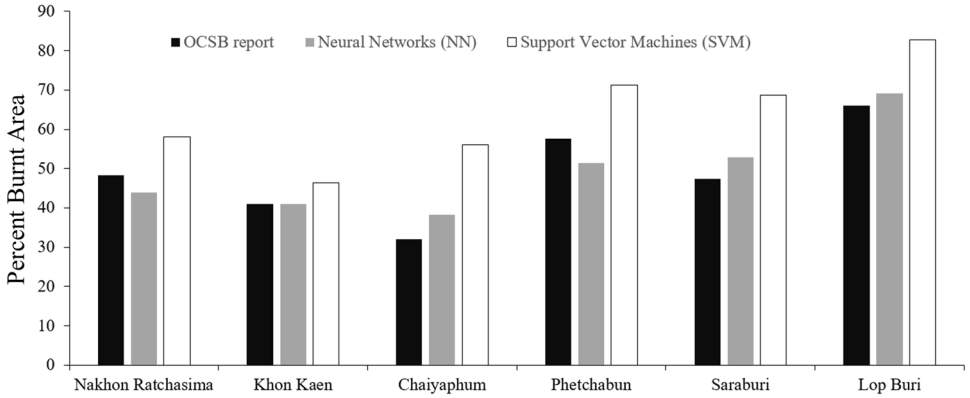

Fig. 9. Comparison of aggregated percent burnt areas by province, determined based on neural network (NN) and support vector machines (SVM) with Office of Cane and Sugar Board (OCSB) of Thailand.

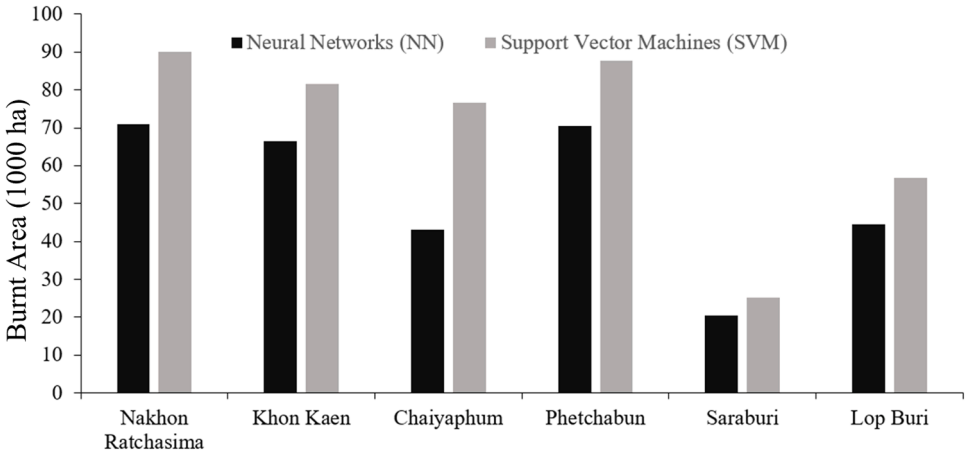

Fig. 10. Comparison of aggregated total burnt areas by province, determined based on neural network (NN) and support vector machines (SVM) with Office of Cane and Sugar Board (OCSB) of Thailand.

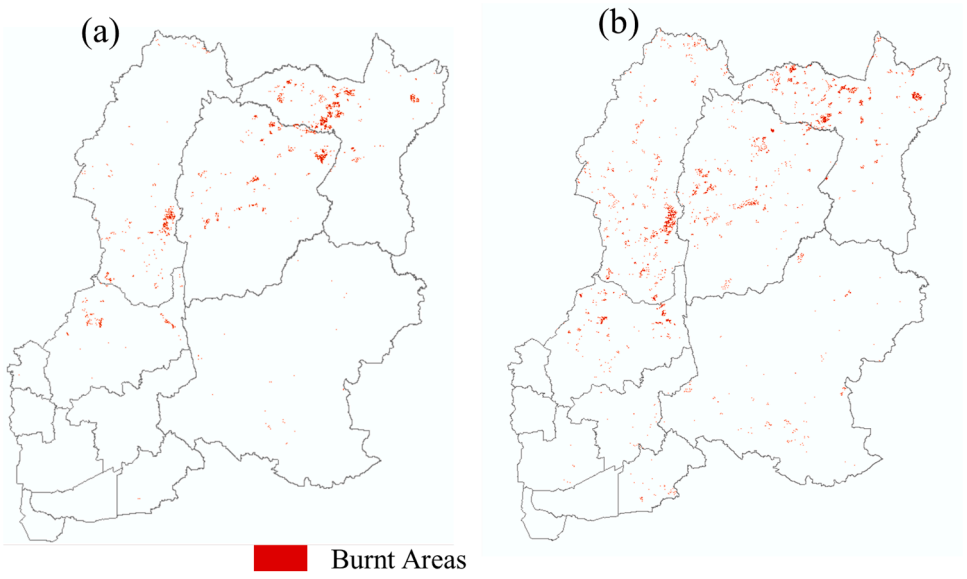

Fig. 11. Burnt areas extracted for Sugarcane pixels from two global products (a) MCD64A1.006 (500 m) (b) FIRECCI51 (~250 m).

reported estimate of 249 thousand ha. The MCD64A1 estimate was 82 % lower while FIRECCI51 estimate was 73 % lower than OCSB's reported burnt area. Little extra burnt area might have resulted due to over-estimation of sugarcane pixels in the sugarcane map. If additional burnt area was excluded, sugarcane burnt areas would have been much lower in both global products. Both NN and SVM methods overestimated while global products underestimated the burnt areas compared to the OCSB reported value. However, both machine learning classifiers showed better agreement with the OCSB report.

Conclusions

Given the need for accurate methods to map crop residue burnt areas and the limited studies on machine learning approaches for this purpose, this study evaluated the performance of two machine learning approaches, support vector machines with different kernel functions, and artificial neural networks, in mapping sugarcane burnt areas in a smallholder farming region located in Central and Northeast Thailand. The major challenge to develop reliable methods for mapping crop residue burnt areas in smallholder farming systems is the lack of crop-specific satellite observations to capture burnt areas' spectral signals. Addressing this issue, reliable sugarcane maps were produced by utilizing frequent observations of sentinel-1 SAR data and Long Short Term Memory (LSTM) deep neural network algorithm. Additionally, the use of harmonized Landsat 8 and Sentinel 2 (HLS) satellite observations with high temporal resolution (4–8 days) helped obtain the required spectral information specific to sugarcane during short burning and harvesting periods, which allowed the development of robust SVM and NN models.

The pixel level evaluation indicated that both SVM and NN methods performed well, achieving an accuracy of over 80 % in identifying sugarcane burnt areas. Among the SVM kernel functions, the Polynomial and Radial Basis Function kernels showed better performance than the linear and sigmoid functions. The NN approach was found to be more accurate than the SVM approach, with an accuracy difference of more than 10 %. The regional scale comparison showed that both NN and SVM estimates captured regional differences in burnt areas, despite some discrepancies in the number of burnt pixels identified by both methods. The SVM method's estimated percent burnt area showed a higher discrepancy (62.90 %) compared to the OCSB reported percentage (48.71 %), while the NN estimate (51.08 %) showed closer agreement with less than 5 % difference. However, the total estimated burnt area showed greater deviation from the OCSB reported value due to

some misclassification errors in the sugarcane mask. Overestimating the sugarcane area in the mask led to higher total estimated burnt areas by both SVM and NN methods. In comparison, the MODIS-based global burnt area products, MCD64A1 and FIRECCI51, substantially underestimated the burnt areas, with a 82 % and 73 % lower estimate than the OCSB report. The machine learning methods developed in this study, particularly the NN method, performed considerably better in terms of capturing spatial trends and total estimated area.

Uncertainties in the regional-scale results from both models could be due to misclassification errors of sugarcane and the approximate harvesting time used in our study. Future studies will aim to improve the sugarcane mask by incorporating a greater number of field observations for labeling land cover types, and produce spatially resolved harvesting timings using satellite data and field observations. The field of machine learning has been evolving rapidly, and new techniques like transformers as well as robust pre-trained deep learning methods such as DeepLab3+ and U-net have shown great promise for many applications such as maturity levels of fruits and crop disease identification [48–50]. We plan to explore these new methods to classify burnt and no-burnt areas. Furthermore, we plan to evaluate the performance of these machine learning models for other crops such as rice and other dominant regions of smallholding farming systems.

Declaration of Competing Interest

The authors declare that they have no known competing financial interests or personal relationships that could have appeared to influence the work reported in this paper.

Data availability

Data will be made available on request.

Acknowledgments

This research is partly funded by the National Aeronautics and Space Administration (NASA), United States NASA-LCLUC Program to the project titled ‘‘Agricultural Land Use Change in Central and Northeast Thailand: Effects on Biomass Emissions, Soil Quality and Rural Livelihoods’’ (Grant number 80NSSC18K0722) and U.S. Department of Agriculture, Agricultural Research Service. USDA is an equal opportunity provider and employer.

References

[1] D. Prato, J. Huertas, Determination of the area affected by agricultural burning, Atmosphere (2019) 10 (Basel).
[2] P. Shyamsundar, N. Springer, H. Tallis, S. Polasky, M. Jat, H. Sidhu, P. Krishnapriya, N. Skiba, W. Ginn, V. Ahuja, J. Cummins, I. Datta, H. Dholakia, J. Dixon, B. Gerard, R. Gupta, J. Hellmann, A. Jadhav, H. Jat, A. Keil, J. Ladha, S. Lopez-Ridaura, S. Nandrajog, S. Paul, A. Ritter, P. Sharma, R. Singh, D. Singh, R. Somanathan, Fields on fire: alternatives to crop residue burning in India, Science 365 (2019) 536. -+.
[3] K. Anderson-Teixeira, S. Davis, M. Masters, E. Delucia, Changes in soil organic carbon under biofuel crops, Global Change Biol. Bioenergy 1 (2009) 75–96.
[4] I. Kumar, V. Bandaru, S. Yampracha, L. Sun, B. Fungtammasan, Limiting rice and sugarcane residue burning in Thailand: current status, challenges and strategies, J. Environ. Manag. 276 (2020).
[5] Valente, F., Laurini, M., 2021. Pre-harvest sugarcane burning: a statistical analysis of the environmental impacts of a regulatory change in the energy sector. 4, 100255.
[6] J. Hall, F. Argueta, L. Giglio, Validation of MCD64A1 and FireCCI51 cropland burned area mapping in Ukraine, Int. J. Appl. Earth Observat. Geoinf. 102 (2021).
[7] L. Giglio, W. Schroeder, C. Justice, The collection 6 MODIS active fire detection algorithm and fire products, Remote Sens. Environ. 178 (2016) 31–41.
[8] K. Lasko, K. Vadrevu, V. Tran, E. Ellicott, T. Nguyen, H. Bui, C. Justice, Satellites may underestimate rice residue and associated burning emissions in Vietnam, Environ. Res. Lett. 12 (2017).
[9] C. Justice, L. Giglio, S. Korontzi, J. Owens, J. Morisette, D. Roy, J. Descloitres, S. Alleaume, F. Petitcolin, Y. Kaufman, The MODIS fire products, Remote Sens. Environ. 83 (2002) 244–262.
[10] S. Escuin, R. Navarro, P. Fernandez, Fire severity assessment by using NBR (Normalized Burn Ratio) and NDVI (Normalized Difference Vegetation Index) derived from LANDSAT TM/ETM images, Int. J. Remote Sens. 29 (2008) 1053–1073.
[11] J. Miller, A. Thode, Quantifying burn severity in a heterogeneous landscape with a relative version of the delta Normalized Burn Ratio (dNBR), Remote Sens. Environ. 109 (2007) 66–80.
[12] M. Deshpande, D. Pillai, M. Jain, Detecting and quantifying residue burning in smallholder systems: an integrated approach using Sentinel-2 data, Int. J. Appl. Earth Observat. Geoinf. 108 (2022).
[13] J. Hall, T. Loboda, L. Giglio, G. McCarty, A MODIS-based burned area assessment for Russian croplands: mapping requirements and challenges, Remote Sens. Environ. 184 (2016) 506–521.
[14] M. Claverie, J. Ju, J. Masek, J. Dungan, E. Vermote, J. Roger, S. Skakun, C. Justice, The harmonized Landsat and sentinel-2 surface reflectance data set, Remote Sens. Environ. 219 (2018) 145–161.
[15] J. Carreiras, S. Quegan, K. Tansey, S. Page, Sentinel-1 observation frequency significantly increases burnt area detectability in tropical SE Asia, Environ. Res. Letters 15 (2020).
[16] D. Gaveau, A. Descals, M. Salim, D. Sheil, S. Sloan, Refined burned-area mapping protocol using Sentinel-2 data increases estimate of 2019 Indonesian burning, Earth Syst. Sci. Data 13 (2021) 5353–5368.
[17] R. Ramo, M. Garcia, D. Rodríguez, E. Chuvieco, A data mining approach for global burned area mapping, Int. J. Appl. Earth Observat. Geoinf. 73 (2018) 39–51.
[18] X. Cao, J. Chen, B. Matsushita, H. Imura, L. Wang, An automatic method for burn scar mapping using support vector machines, Int. J. Remote Sens. 30 (2009) 577–594.
[19] E. Dragozi, I. Gitas, D. Stavrakoudis, J. Theocharis, Burned area mapping using support vector machines and the FuzCoC feature selection method on VHR IKONOS imagery, Remote Sens. 6 (2014) 12005–12036 (Basel).
[20] G. Petropoulos, C. Kontoes, I. Keramitsoglou, Burnt area delineation from a uni-temporal perspective based on Landsat TM imagery classification using Support Vector Machines, Int. J. Appl. Earth Observat. Geoinf. 13 (2011) 70–80.
[21] P. Brivio, M. Maggi, E. Binaghi, I. Gallo, Mapping burned surfaces in sub-Saharan Africa based on multi-temporal neural classification, Int. J. Remote Sens. 24 (2003) 4003–4018.
[22] M. Gimeno, J. San-Miguel-Ayanz, Evaluation of RADARSAT-1 data for identification of burnt areas in Southern Europe, Remote Sens. Environ. 92 (2004) 370–375.
[23] I. Gomez, M. Martin, Prototyping an artificial neural network for burned area mapping on a regional scale in Mediterranean areas using MODIS images, International J. Appl. Earth Observat. Geoinf. 13 (2011) 741–752.
[24] G. Petropoulos, K. Vadrevu, G. Xanthopoulos, G. Karantounias, M. Scholze, A comparison of spectral angle mapper and artificial neural network classifiers combined with Landsat TM imagery analysis for obtaining burnt area mapping, Sensors 10 (2010) 1967–1985.
[25] M. Pinto, R. Libonati, R. Trigo, I. Trigo, C. DaCamara, A deep learning approach for mapping and dating burned areas using temporal sequences of satellite images, Isprs J. Photogramm. Remote Sens. 160 (2020) 260–274.
[26] K. Chaibandit, S. Konyai, D.C. Slack, Evaluation of the water footprint of sugarcane in eastern Thailand, Eng. J. 21 (5) (2017) 193–201.
[27] Athipanyakul, T., K. Choonhwong., C. Potchanasin. 2020. The challenge for Thai sugarcane farmers. Available at https://ap.fftc.org.tw/article/1840 (accessed on Oct 23, 2022).
[28] B.E. Boser, I.M. Guyon, V.N. Vapnik, A training algorithm for optimal margin classifiers, in: Proceedings of the 5th Annual ACM Workshop on Computational Learning Theory, Pittsburgh 5, 1992, pp. 144–152.
[29] V. Vapnik, The Nature of Statistical Learning Theory, Springer-Verlag, New York, 1995.
[30] V Vapnik, Statistical Learning Theory, Wiley, N.Y, 1998.
[31] S. Haykin, Neural Networks: a Comprehensive Foundation, PTR, Prentice Hall, 1994.
[32] F. Rosenblatt, The perceptron: a probabilistic model for information storage and organization in the brain, Psychol. Rev. 65 (6) (1958) 386.
[33] D. Cox, T. Dean, Neural networks and neuroscience-inspired computer vision, Curr. Biol. 24 (2014) R921–R929.
[34] S. Kaushik, M. Kumar, H. Arabnia, Natural language translation system using neural networks. Ic-Ai’2001, in: Proceedings of the International Conference on Artificial Intelligence Vols I-Iii, 2001, pp. 1073–1080.
[35] S. Dhanjal, Artificial neural networks in speech processing: problems & challenges, in: 2001 IEEE Pacific Rim Conference on Communications, Computers and Signal Processing, Vols I and Ii, Conference Proceedings, 2001, pp. 510–513.
[36] R. Yaramasu, V. Bandaru, K. Pnvr, Pre-season crop type mapping using deep neural networks, Comput. Electron. Agricult. 176 (2020).
[37] NASA Shuttle Radar Topography Mission (SRTM), 2013. Shuttle radar topography mission (SRTM) Global. distributed by opentopography. 10.5069/G9445JDF. Accessed: 2023-03-21.
[38] D. Bolton, J. Gray, E. Melaas, M. Moon, L. Eklundh, M. Friedl, Continental-scale land surface phenology from harmonized Landsat 8 and Sentinel-2 imagery, Remote Sens Environ (2020) 240.
[39] J. De Leeuw, H. Jia, L. Yang, X. Liu, K. Schmidt, A. Skidmore, Comparing accuracy assessments to infer superiority of image classification methods, Int. J. Remote Sens. 27 (2006) 223–232.
[40] C. Kontoes, H. Poilve, G. Florsch, I. Keramitsoglou, S. Paralikidis, A comparative analysis of a fixed thresholding vs. a classification tree approach for operational

burn scar detection and mapping, Int. J. Appl. Earth Observat. Geoinf. 11 (2009) 299–316.
[41] Office of Cane and Sugar Board (OCSB), Report of the Comparison of Sugarcane and Sugar Production Efficiency of Sugar Factories in Thailand in the Production Year 2019/20, Office of Cane and Sugar Board (OCSB), Bangkok, Thailand, 2020. Available online: http://www.sugarzone.in.th. accessed on October 12, 2022.
[42] C. Huang, L. Davis, J. Townshend, An assessment of support vector machines for land cover classification, Int. J. Remote Sens. 23 (2002) 725–749.
[43] B. Yekkehkhany, A. Safari, S. Homayouni, M. Hasanlou, F. Karimipour, R. Abbaspour, A comparison study of different kernel functions for SVM-based classification of multi-temporal polarimetry SAR data, 1st Isprs Int. Conf. Geospat. Inf. Res. 40 (2014) 281–285.
[44] Y. Shao, R. Lunetta, Comparison of support vector machine, neural network, and CART algorithms for the land-cover classification using limited training data points, Isprs J. Photogr. Remote Sens. 70 (2012) 78–87.
[45] Li, Y., Feng, Z., Chen, S., Zhao, Z., Wang, F., 2020. Application of the artificial neural network and support vector machines in forest fire prediction in the Guangxi Autonomous Region, China. Discrete Dynamics in Nature and Society 2020.
[46] E. Raczko, B. Zagajewski, Comparison of support vector machine, random forest and neural network classifiers for tree species classification on airborne hyperspectral APEX images, Eur. J. Remote Sen. 50 (2017) 144–154.
[47] Chuvieco, E., Pettinari, M.L., Lizundia-Loiola, J., Storm, T., Padilla Parellada, M., 2018. ESA fire climate change initiative (Fire_cci): MODIS Fire_cci burned area pixel product, version 5.1. Centre for environmental data analysis, 10.5285/58f00d8814064b79a0c49662ad3af537.
[48] K. Bose, K. Shubham, V. Tiwari, K.S. Patel, Insect Image Semantic Segmentation and Identification Using UNET and DeepLab V3+, Springer Nature Singapore, Singapore, 2023, pp. 703–711.
[49] C. Cai, J. Tan, P. Zhang, Y. Ye, J. Zhang, Determining strawberries' varying maturity levels by utilizing image segmentation methods of improved DeepLabV3 +, Agronomy 12 (2022).
[50] K. Li, W. Zhao, R. Peng, T. Ye, Multi-branch self-learning vision transformer (MSViT) for crop type mapping with Optical-SAR time-series, Comput. Electron. Agricult. 203 (2022), 107497.